AIRCRAFT WING ANTI-ICING: THERMAL BOUNDARY-LAYER MODELS COMPARISON

Guilherme Araújo Lima da Silva[1], Otávio de Mattos Silvares[1,2],Euryale Jorge Godoy de Jesus Zerbini[1]
[1]Escola Politécnica da Universidade de São Paulo, São Paulo, Brazil
[2]Instituto Mauá de Tecnologia, São Caetano, Brazil

Abstract

Based on a tested electro-thermal anti-ice numerical tool, the present authors propose simplifications in model assumptions to assess their relevance in wing surface temperatures prediction and end of runback water location. The purpose is to demonstrate that momentum and heat analogy and abrupt laminar-turbulent transition approximations may not represent the physical phenomena with the accuracy required. The existent mathematical model considers flow around non-isothermal and transpired airfoil surfaces with a smooth laminar-turbulent transition occurence. Two simplifications are implemented herein: 1) the flow over isothermal surfaces by the use of Colburn analogy; 2) the abrupt laminar-turbulent transition. The boundary layer procedures used in classic icing codes assume similar simplifications and they have limited application in wing electro-thermal anti-ice simulation. The present paper results show that streamwise surface temperature gradient and the occurence of transition, within the protected area, must be considered in mathematical modelling of aircraft thermal ice protection.

1 Introduction

The ice accretion on wings and horizontal stabilizers may cause aerodynamic performance degradation, weight increase, flight control difficulties and, in critical cases, may lead to operational safety margins reduction. When aircraft flies through supercooled water droplets clouds, which are in meta-stable equilibrium, ice will form in all surfaces that are subjected to impingement and not protected. Usually, thermal ant-ice systems are designed, developed and certified with support of a numerical tool. Under icing conditions, it is necessary to heat and control the temperature of the airfoil surface at leading edge region to prevent ice formation. The heating system balances the cooling effects caused by coupled convection heat and mass transfer imposed by the air flow loaded with supercooled water droplets and the runback water flow over airfoil.

With a thermal anti-ice activated, the water droplets impinge and spreads over the leading edge region. Then the runback water flows to downstream regions driven by pressure and shear forces applied by external flow around the airfoil. If a critical thickness is reached, the water film breaks-up and forms rivulets. The change from film to rivulets flow pattern is marked by a decrease in wetted area. The dry patches start to grow between rivulets and the airfoil surface becomes directly exposed to gaseous flow around airfoil.

Currently, the electro-thermal anti-ice systems are in the aerospace industry focus due to advent of more electric airplane or even the bleedless system architectures, where all the power is provided by an electrical generator and not by high pressure and temperature engine bleed air. Silva et al. (2007a) reviewed the literature and also the icing and anti-icing numerical tools mathematical models and capabilities. Many works applied the momentum and heat tranfer analogy to icing airfoils (Wright, 1995; Guffond and Brunet, 1988; Gent, 1990; Wright et al., 1997) and assumed an abrupt laminar-turbulent transition. Usually they consider airfoil or ice surfaces as isothermal, non-permeable and fully rough. However, few researchers applied the momentum and thermal boundary layer integral models to anti-ice simulation with success. Morency et al. (1999) developed the numerical code CANICE A that evaluates the heat transfer

coefficient considering laminar flow over isothermal surface(Smith and Spalding, 1958), turbulent flow over smooth and non-isothermal surface(Ambrok, 1957) and abrupt laminar-turbulent transition. Same authors developed other version of the code, CANICE B, and use the experimental data of heat transfer coefficient . Only this second code represented satisfactorily the surface temperature numerical results. Henry (1989) transient ice protection code applied the Makkonen (1985) boundary-layer model that, which, in turn, is used in ONERA2D icing code(Guffond and Brunet, 1988). Al-Khalil et al. (2001) employed experimental data in his ANTICE code simulations. Neither LEWICE (Wright, 1995) nor ANTICE heat transfer coefficients were used in validation process. Gent et al. (2003) reported difficulties when applying TRAJICE2 boundary layer model(Gent, 1990; Gent et al., 2000; Makkonen, 1985) to rotorcraft ice protection systems. The authors got overestimated results and recommended more research about heat transfer coefficient evaluation(Gent et al., 2003).

2 Objective

The objective of the present paper is to compare convective heat transfer modeling strategies and assess their relevance for accurate temperature distribution and runback water evaporation prediction. The purpose is to demonstrate that non-isothermal and smooth laminar-transition assumptions are important when applying boundary-layer integral analysis to thermal anti-ice performance simulation. Two simplifications, which are commonly adopted by aerospace industry and researchers, are implemented herein: 1) the flow over isothermal surfaces by the use of Colburn analogy; 2) the abrupt laminar-turbulent transition. Each simplification is implemented and tested separately to check if that numerical code assumption will change predictions of temperature, heat transfer and runback water end position.

3 Mathematical Models

The present paper uses the anti-ice thermal model developed by Silva et al. (2007a,b), whom briefly described the mathematical model, presented some numerical code results and compared with experimental data as well as other codes results. The anti-ice system operation simulation applies the First Law of Thermodynamics to liquid water flow and solid airfoil surface together the Conservation of Mass and Momentum to liquid water flow. The wetness factor estimation, by water film breakdown and rivulets formation, was based in other work (Silva et al., 2006) plus the assumption of constant rivulets spacing. Their model requires solution of : I) velocity and pressure fields around the airfoil; II) droplet trajectories; III) momentum and thermal boundary layers to obtain the coupled heat and mass transfer over the airfoil solid surface and liquid water flow; IV) First Law of Thermodynamics to the liquid water and airfoil solid surface plus the Conservation of Mass and Momentum to the liquid water flow (film and rivulets) over the airfoil. Both flow field around airfoil and local collection efficiency data were provided by external numerical codes (I and II). The momentum and thermal boundary-layer are evaluated (III) in order to estimate the heat and mass transfer around airfoil over non-isothermal and transpired surfaces with a smooth laminar-turbulent transition occurrence (Silva et al., 2007a). With data from previous steps (I, II and III), the anti-ice mathematical model (IV) is able to predict operational parameters like solid surface temperatures, runback mass flow rate and convection heat transfer coefficient distributions along the airfoil solid surface. The thermal (IV) and boundary-layer (III) models have been applied to thermal anti-ice system operation simulation since works of Silva (2002); Silva et al. (2003).

The present paper presents the original thermal boundary-layer model (III) and the proposed simplifications. The changes were implemented one by time. All the other other original models (I, II and IV) are kept the same.

3.1 Thermal Boundary-Layer - Non-isothermal Model

Silva et al. (2007a) adopted an boundary-layer integral analysis that considers flow over non-isothermal surfaces. At stagnation point, the local convective heat transfer is estimated by isothermal integral analysis developed by Smith and Spalding (1958):

$$\mathrm{Nu}_0 = \left[0.246 \cdot \mathrm{Re}_\infty \cdot \left. \frac{d\left(u_e/V_\infty\right)}{d\left(s/c\right)} \right|_{s=s_0} \right]^{1/2} \tag{1}$$

Ambrok (1957) developed an original expression in order to evaluate laminar local convective heat transfer due to a flow over non-isothermal surfaces with moderate pressure gradient:

$$\mathrm{Nu}_{lam} = 0.3 \cdot \mathrm{Re}_s \cdot \Delta T \cdot \left(\int_{s_0}^{s_{Star}} \frac{u_e \cdot \Delta T^2}{\nu_{air}} \, ds \right)^{-1/2} \tag{2}$$

The evaluation of $\Delta_{2,turb}$ by equation (5) requires the knowledge of $\Delta_{2,lam}$ value at onset transition location as initial condition. By using Ambrok (1957) developments in turbulent regime, the $\Delta_{2,turb}$ is estimated:

$$\mathrm{Re}_{\Delta_{2,lam}} = \frac{0.83}{\Delta T} \cdot \left(\int_{s_{stag}}^{s_{tr}} \frac{u_e \cdot \Delta T^2}{\nu_{air}} \, ds \right)^{1/2} \tag{3}$$

The local convective heat transfer in turbulent regime is evaluated by Ambrok (1957):

$$\mathrm{St}_{turb} = 0.0125 \cdot \mathrm{Re}_{\Delta_{2,turb}}^{-0.25} \cdot \mathrm{Pr}^{1/2} \tag{4}$$

Alike Narasimha (1990), the present paper assumes that the virtual origin of turbulent boundary coincides with the transition onset, where the turbulent spots start to appear. It is assumed that inttermitency γ and enthalpy thickness $\Delta_{2,turb}$ start to be different than zero at transition onset s_{tr}. Therefore, the turbulent enthalpy thickness is:

$$\mathrm{Re}_{\Delta_{2,turb}} \cdot \Delta T = \left[0.0156 \cdot \mathrm{Pr}^{-1/2} \cdot \mu_{air}^{-1} \cdot \int_{s_{tr}}^{s} G \cdot \Delta T^{1.25} ds + \left(\mathrm{Re}_{\Delta_{2,tr}} \cdot \Delta T_{tr} \right)^{1.25} \right]^{0.8} \tag{5}$$

3.2 Thermal Boundary-Layer - Isothermal Model

Classic icing codes (Wright et al., 1997) use the integral analysis to evaluate laminar heat transfer around icing airfoils (Smith and Spalding, 1958). Flow over isothermal surfaces is an acceptable assumption for non-heated airfoils subjected to ice formation, since the exposed ice or airfoil surface equilibrium temperatures are aproximately constant. In this model, the heat transfer coefficient $h_{air,lam}$ is estimated by evaluating the laminar conduction thickness $\Delta_{4,lam}$:

$$\frac{u_e^{2.87}}{\nu} \cdot \Delta_{4,lam}^2 = 11.68 \cdot \int_{s_0}^{s} u_e^{1.87} ds \qquad \text{and} \qquad \Delta_{4,lam} = \frac{k_{air}}{h_{air,lam}} \tag{6}$$

In turbulent regime, the classic icing codes evaluate the heat transfer coefficient by assuming flow over a fully rough surface and one of heat and momentum transfer analogies. As there is no ice on the airfoil when operating an anti-ice system, the present paper assumes flow over a smooth surface and the *Colburn* analogy to estimate:

$$\mathrm{St}_{turb} \cdot \mathrm{Pr}^{2/3} = \frac{C_{f,turb}}{2} \qquad \text{and} \qquad \frac{C_{f,turb}}{2} = 0.0125 \cdot \mathrm{Re}_{\delta_{2,turb}}^{-0.25} \tag{7}$$

For the present work, the integral equation of momentum thickness in turbulent regime is simplified to (Kays and Crawford, 1993):

$$\delta_{2,turb} = \left[\frac{0.0156 \cdot \nu_{air}^{1/4}}{u_e^{4.11}} \cdot \int_{s_{tr}}^{s} u_e^{3.86}\, ds + (\delta_{2,tr})^{5/4} \cdot (\frac{u_{e,tr}}{u_e})^{4.11} \right]^{4/5} \tag{8}$$

At position s_{tr}, both intermittency and $\delta_{2,tr}$ begin to be greater than zero (Narasimha, 1990). With momentum thickness, $\mathrm{Re}_{\delta_{2,turb}}$ is obtained to allow evaluation of $C_{f,turb}$ and St_{turb}.

3.3 Laminar-Turbulent Transition - Intermittency Model

Silva et al. (2007a) adopted the work of Reynolds et al. (1958b) that defines the laminar-turbulent transition region statistically by a mean position s_m and a standard deviation length σ. Both St and C_f within transition region are calculated by linear combination of the laminar $C_{f,lam}$ and St_{lam} with turbulent $C_{f,turb}$ and St_{turb} values.
Within the laminar-turbulent transition region, the St number is estimated by:

$$\mathrm{St}(s) = \begin{cases} \mathrm{St}_{lam}(\mathrm{Re}_s) & s < s_m - 2 \cdot \sigma \\ [1 - \gamma(s)] \cdot \mathrm{St}_{lam}(\mathrm{Re}_s) + \gamma(s) \cdot \mathrm{St}_{turb}(\mathrm{Re}_s) & s \geq s_m - 2 \cdot \sigma \end{cases} \tag{9}$$

Similarly, the linear combination procedure is also applied to friction coefficient calculation C_f, i.e., the $\mathrm{St}(s)$ is replaced by $C_f(s)$ in equation (9). The turbulent flow probability $\gamma(\mathrm{Re}_s)$ is evaluated by:

$$\gamma(\mathrm{Re}_s) = \int_{-\infty}^{\mathrm{Re}_s} \left(\frac{1}{\mathrm{Re}_s} \cdot \sqrt{2 \cdot \pi} \right) \cdot \exp\left(-\frac{\mathrm{Re}_s - \mathrm{Re}_{s_m}^2}{2 \cdot \mathrm{Re}_\sigma^2} \right) d(\mathrm{Re}_s) \tag{10}$$

3.4 Laminar-Turbulent Transition - Abrupt Model

As reported by (Wright et al., 1997) , the classic icing codes assume that the laminar-turbulent transition region has a very short length, i.e., the flow is turbulent just after the onset occurence. However, Pimenta (1975) and Bragg et al. (1996) observed no evidences of abrupt transition occurence in flow over fully rough flat plates or airfoils. Stefanini et al. (2007) demonstrated that transition parameters region variation, such as onset and length, affects ice shape significantly. Moreover, Gelder and Lewis (1951) and Sogin (1954) concluded that laminar-turbulent transition is also important in thermal ice protection design. Despite of lack of evidences, this assumption is commonly adopted by aerospace engineers to develop aircraft anti-ice systems.

4 Experimental Data

Al-Khalil et al. (2001) performed anti-icing experiments at Icing Research Tunnel at NASA Glenn Research Center facilities, Cleveland, Ohio, USA, by measuring surface temperature and overall heat transfer coefficient in order to validate ANTICE numerical code. The airfoil tested was 1.828 m span by 0.914 m chord NACA 0012 profile with electronically controlled heaters. Each heater element in streamwise direction had one thermocouple, one thermoresistor sensor and one heat flux gauge installed. The 22A is an evaporative and 67A is a wet case. In 22A case, freestream velocity is 44.7 m/s, total temperature is -7.6 °C, liquid water content is 0.78 g· m^{-3}. Case 67A has freestream velocity 89.4 m/s, total temperature -21.6 °C, liquid water content 0.55 g· m^{-3}. Both cases have 20 μm as median volumetric diameter and 0 as angle of attack.

5 Results

Figure 1(a) presents the solid surface temperature distributions estimated by using the non-isothermal, which is the baseline, and isothermal boundary-layer models. All the other assumptions and models are the same. Only the hypothesis of non-isothermal surface was changed.

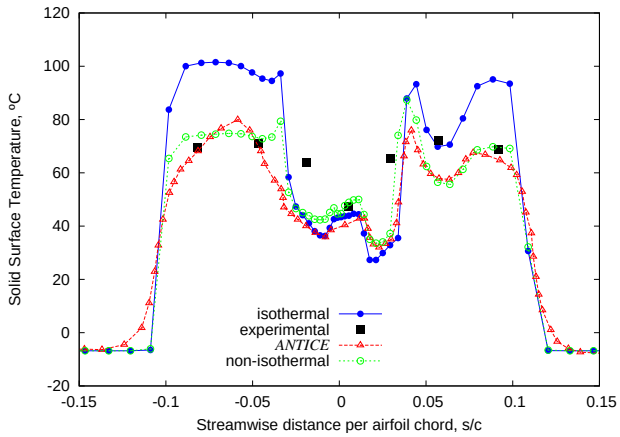

(a) Non-isothermal and isothermal

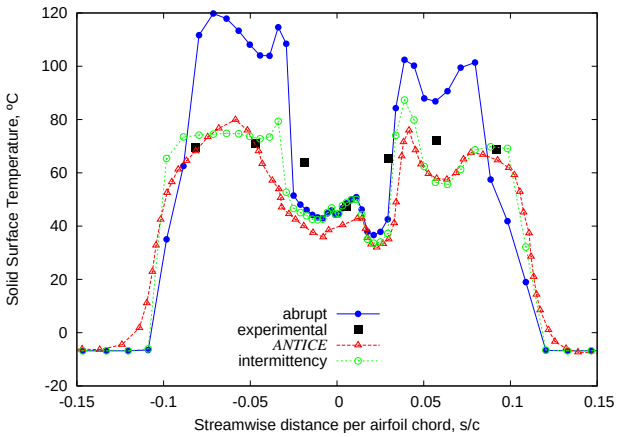

(b) Smooth and abrupt transition

Figure 1: Case 22A - Present paper temperature results compared with experimental data and ANTICE results (Al-Khalil et al., 2001)

The predictions are compared with experimental data and ANTICE numerical results (Al-Khalil et al., 2001). On the other hand, Figure 1(b) presents temperature predictions when adopting intermittency and abrupt transition. The abrupt transition was fixed at the mean position of transition region, s_m, of the baseline model, which are located in $s/c = 0.08$ and -0.083 for case 22A. The transition standard deviation, σ, was set as 0.04 at s/c for case 22A. The estimated temperature effects caused by boundary-layer assumptions for case 67A are shown in Figures 3(a) and 3(b). In both 22A and 67A cases, the baseline model, which adopts non-isothermal and inttermitency models, estimated temperatures closer to experimental data and ANTICE numerical results than the isothermal and abrupt transition models.

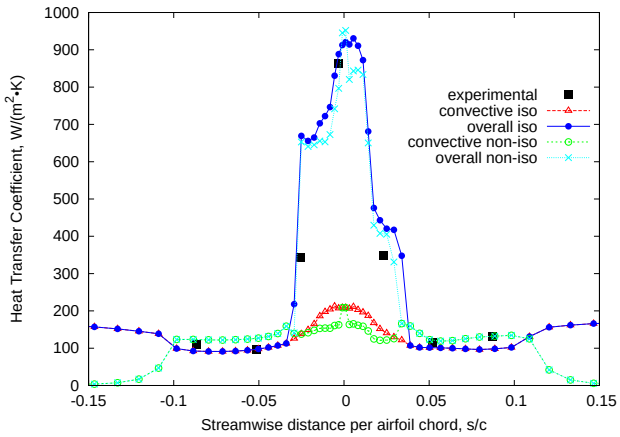

(a) Non-isothermal and isothermal

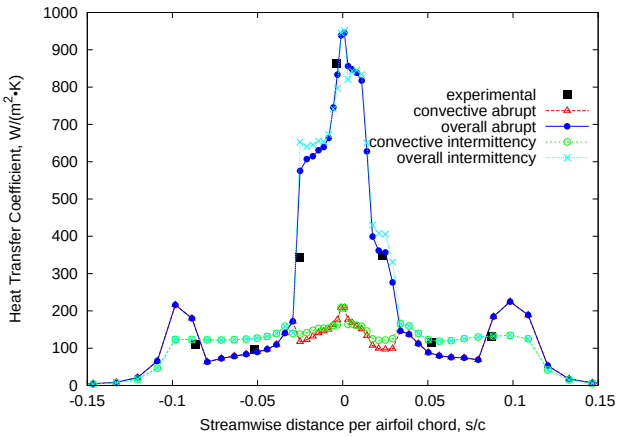

(b) Smooth and abrupt transition

Figure 2: Case 22A - Present paper overall and convective heat transfer coefficient results compared with experimental data (Al-Khalil et al., 2001)

The overall heat transfer coefficient considers effects of convection, evaporation and runback water enthalpy flow as well as water impigement enthalpy and momentum. Therefore, when the surface is dry, the overall is equal to convective heat transfer coefficient . On the other hand, when the surface is wetted by water film or rivulets, the overall is greater than convective. This fact indicates mainly that the heat transfer is enhanced due to evaporative cooling. Figure 2(a) shows that isothermal model has negligible variations in due to thermodynamic properties variations and is symmetrical. On the other hand, the non-isothermal model presents significant

variations at leading edge. As expected, the non-isothermal model predicted higher values of heat transfer coefficient at turbulent region due to increase of temperature difference (between solid wall and ambient) at end of water filme. Other clear difference is at end of protected area, where the flow is turbulent, the non-isothermal model estimates a decrease in while the isothermal a increase. Those effects were researched extensively by Reynolds et al. (1958a) in heated flat plates operating in dry air tunnel.

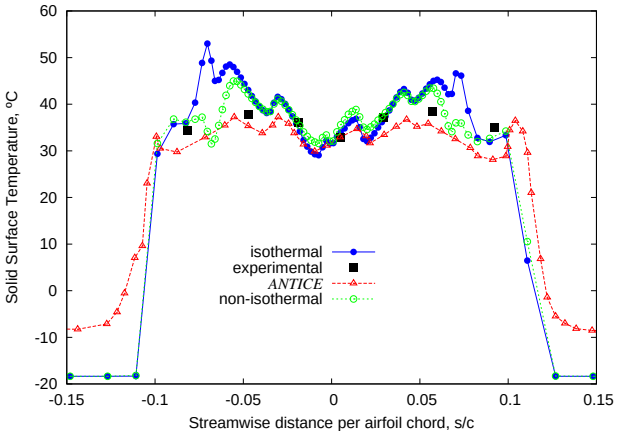

(a) Non-isothermal and isothermal

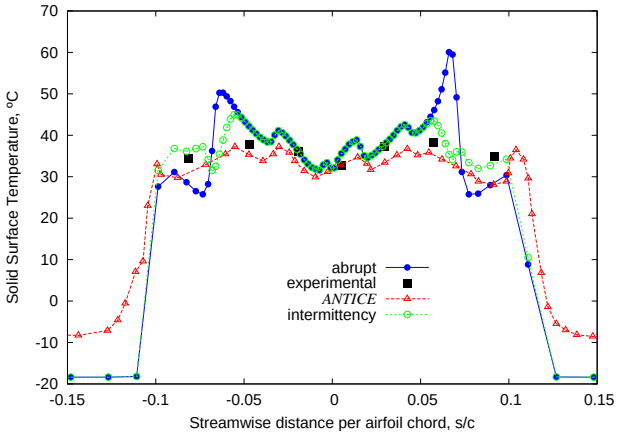

(b) Smooth and abrupt transition

Figure 3: Case 67A - Present paper temperature results compared with experimental data and ANTICE results (Al-Khalil et al., 2001)

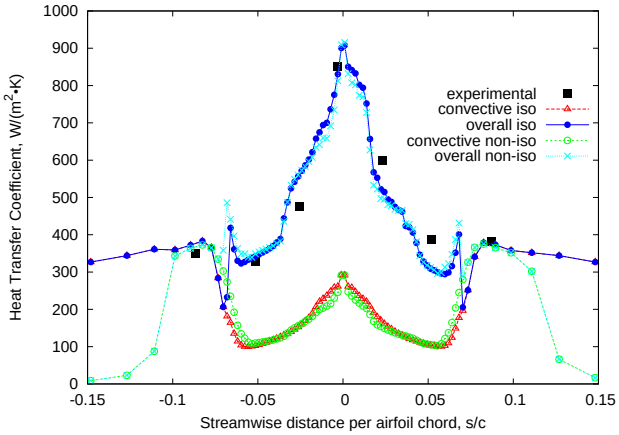

(a) Non-isothermal and isothermal

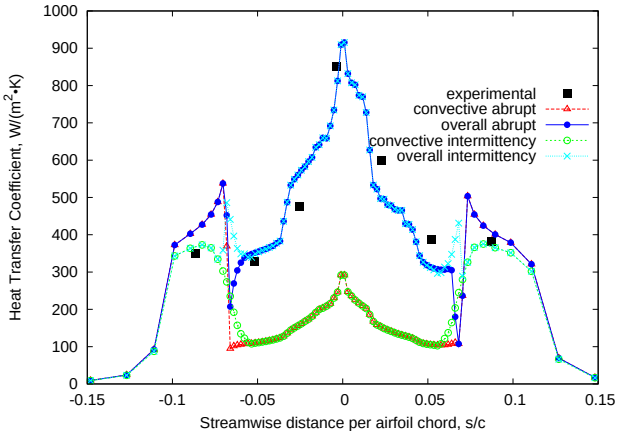

(b) Smooth and abrupt transition

Figure 4: Case 67A - Present paper overall and convective heat transfer coefficient results compared with experimental data (Al-Khalil et al., 2001)

The abrupt transition was fixed at the mean position of transition region, which are $s/c = 0.07$ and -0.067 in case 67A. The transition σ was set to 0.007 for case 67A in both upper and lower surfaces. The transition parameters (s_m and σ) were found by matching the baseline model estimation with experimental data for overall heat transfer coefficient. Those values were not changed in isothermal nor abrupt model runs. Figure 4(a) shows a sharp increase of convective heat transfer in abrupt model while the intermittency model predicted a smoother curve and closer to experimental data. Due to more constant temperature distribution in case 67A than 22A, there are small deviations in the convective heat transfer coefficient predicted by non-isothermal and isothermal models. Except at the region of end of water flow and end of

heated area, both models behave similarly. A sharp increase and a overshoot of is observed in abrupt transition model results that is shown in Figure 4(b). This fact caused the instaneous evaporation of all water and, thus, a local temperature increase.
For case 22A, all the models (non-isothermal and isothermal, abrupt and smooth transition) predicted runback water evaporation at streamwise position $s/c = 0.024$ in both upper and lower surfaces. But, in case 67A, the baseline model (non-isothermal and smooth transition) provided $s/c = 0.077$ and $s/c = -0.073$ as water disappearing positions. Isothermal model resulted in $s/c = 0.07$ and $s/c = -0.068$ positions. By considering abrupt transition, the positions changed to $s/c = 0.066$ and $s/c = -0.068$. The changes are significant when compared with the total protected area, which is located between $s/c = -0.102$ and 0.113.

6 Conclusions

The heated airfoil operating under icing conditions has some important characteristics that differenciates the problem from the case of adiabatic airfoil subjected to ice growth. In presence of thermal ice protection, the usual boundary-layer hypotheses assumed by classic codes does not represent the physical phenomena satisfactorily for engineering purposes. The streamwise surface temperature gradient and the occurence of transition, within the protected area, must be considered in the mathematical modelling. Depending on the onset position and length of transition region, the laminar flow may cover a significant area when compared to fully turbulent flow area and vice-versa. Moreover, a local parameter prediction is much more sensitive to punctual variations than an integral that is averaged over a surface. Therefore, heat transfer coefficient streamwise variations, induced either by transition or surface temperature gradient, may have great impact on surface temperature, evaporation mass flux and runback water distributions.

Acknowledgment

G. A. L. da Silva wish to acknowledge Fundação de Amparo à Pesquisa do Estado de São Paulo (FAPESP) for the financial support received by the doctoral grant 07/00419-0.

References

Al-Khalil, K. M., Horvath, C., Miller, D. R. and Wright, W., 2001, Validation of nasa thermal ice protection computer codes. part 3 - validation of antice, *Contractor Report 2001-210907*, NASA, Cleveland, OH.

Ambrok, G. S., 1957, Approximate solution of equations for the thermal boundary layer with variations in boundary layer structure, *Soviet Physics - Technical Physics* (2), 1979–86.

Bragg, M. B., Cummings, S. L. and Henze, C. M., 1996, Boundary-layer and heat transfer measurements on an airfoil with simulated ice roughness, *AIAA Paper 96-0866*, Aerospace Sciences and Meeting, 34., 1996, Reno, America Institute of Aeronautics and Astronautics, Reston, pp. 1–16.

Gelder, T. F. and Lewis, J. P., 1951, Comparison of heat transfer from airfoil in natural and simulated icing conditions, *Technical Note 2480*, NACA, Washington.

Gent, R., 1990, Trajice2 - a combined water droplet trajectory and ice accretion prediction program for aerofoils, *Technical Report 90054*, RAE, Farnborough.

Gent, R., Moser, R., Cansdale, J. and Dart, N., 2003, The role of analysis in the development of rotor ice protection system, *SAE Paper 2003-01-2090*, FAA In-flight Icing, Ground De-icing International Conference & Exhibition, 1., Chicago, 2003, IL, Society of Automotive Engineers, Warrendale.

Gent, R. W., Dart, N. P. and Cansdale, J., 2000, Aircraft icing, *Phil. Trans. Royal Society London A* **n.a.**(358), 2873–2911.

Guffond, D. and Brunet, L., 1988, Validation du programme bidimensionnel de capitation, *Rapport Technique RP 20/5146 SY*, ONERA, Châtillon Cedex, France.
Henry, R., 1989, *Etude du fonctionnement d'un degivreur electrique : modelisation et mesure en soufflerie givrante de temperature parietale par thermographie infrarouge*, PhD thesis, Blaise Pascal Université, Clemont-Ferrand.
Kays, W. M. and Crawford, M. E., 1993, *Convective heat and mass transfer*, McGraw-Hill, New York.
Makkonen, L., 1985, Heat transfer and icing of a rough cylinder, *Cold Regions and Technology* **10**, 105–116.
Morency, F., Tezok, F. and Paraschivoiu, I., 1999, Heat and mass transfer in the case of an anti-icing system modelisation, *AIAA Paper 99-0623*, Aerospace Sciences Meeting and Exhibit, 37., 1999, Reno, American Institute of Aeronautics and Astronautics, Reston.
Narasimha, R., 1990, Modelling the transitional boundary layer, *Contractor Report 187487*, NASA, Washington.
Pimenta, M. M., 1975, *The turbulent boundary layer: an experimental study of the transport of momentum and heat with the effects of roughness*, PhD thesis, Stanford University, Stanford.
Reynolds, W. C., Kays, W. M. and Kline, S. J., 1958a, Heat transfer in the turbulent incompressible boundary layer. III - Arbitrary wall temperature and heat flux, *Memorandum 12-3-58W*, NACA, Washington, D.C.
Reynolds, W. C., Kays, W. M. and Kline, S. J., 1958b, Heat transfer in the turbulent incompressible boundary layer. iv - effect of location of transtion and prediction of heat transfer in a known transition region, *Memorandum 12-4-58W*, NACA, Washington, D.C.
Silva, G. A. L., 2002, *Modelagem e simulação da operação de sistema antigelo eletrotérmico de um aerofólio*, Master's thesis, Escola Politécnica da Universidade de São Paulo, São Paulo, SP, Brazil.
Silva, G. A. L., Silvares, O. M. and Zerbini, E. J. G. J., 2003, Airfoil anti-ice system modeling and simulation, *AIAA Paper 2003-734*, 41st Aerospace Sciences Meeting and Exhibit, 2003, Reno, America Institute of Aeronautics and Astronautics, Reston.
Silva, G. A. L., Silvares, O. M. and Zerbini, E. J. G. J., 2006, Water film breakdown and rivulets formation effects on thermal anti-ice operation simulation, *AIAA Paper 2006-3785*, AIAA/ASME Joint Thermophysics and Heat Transfer Conference, 9., 2006, San Francisco, America Institute of Aeronautics and Astronautics, Reston.
Silva, G. A. L., Silvares, O. M. and Zerbini, E. J. G. J., 2007a, Numerical simulation of airfoil thermal anti-ice operation. Part 1: Mathematical modeling, *Journal of Aircraft* **44**(2), 627–33.
Silva, G. A. L., Silvares, O. M. and Zerbini, E. J. G. J., 2007b, Numerical simulation of airfoil thermal anti-ice operation. part 2: Implementation and results, *Journal of Aircraft* **44**(2), 634–41.
Smith, A. G. and Spalding, D. B., 1958, Heat transfer in a laminar boundary layer with constant fluid properties and constant wall temperature, *Journal of the Royal Aeronautical Society* **62**, 60–64.
Sogin, H. H., 1954, A design manual for thermal anti-icing systems, *Technical Report 54-13*, Wright Air Development Center Technical, Illinois.
Stefanini, L. M., Silvares, O. M., Silva, G. A. L. and Zerbini, E. J. G. J., 2007, Convective heat transfer effects in airfoil icing, *Procedings of COBEM 2007*, 19th International Congress of Mechanical Engineering, Brazilian Society of Mechanical Sciences and Engineering, Rio de Janeiro.
Wright, W. B., 1995, User manual for the improved nasa lewis ice accretion code lewice 1.6, *Contractor Report 198355*, NASA, Cleveland.
Wright, W., Gent, R. and Guffond, D., 1997, Dra/nasa/onera collaboration on icing research part ii - prediction of airfoil ice accretion, *Contractor Report 202349*, NASA, Cleveland.